Original Article

Institution of MECHANICAL ENGINEERS

Journal of RAIL AND RAPID TRANSIT

Proc IMechE Part F:
J Rail and Rapid Transit
0(0) 1–8

DOI: 10.1177/0954409715616997
pif.sagepub.com

SAGE

Quantification of the lateral forces in concrete sleeper fastening systems

Brent A Williams, Donovan Holder, J Riley Edwards, Marcus S Dersch and Christopher PL Barkan

Abstract

Consistent increases in cumulative freight tonnages, combined with the move towards increased higher-speed intercity passenger rail operation, have placed greater demands on North American railroad infrastructure. Concrete sleepers and fastening system components are known to fail at a wide range of life cycle intervals when subjected to demanding loading environments. Such failures can cause track geometry defects, require repetitive maintenance procedures, and present critical engineering challenges. Rail seat deterioration, the degradation of the concrete material beneath the rail, has been identified through a survey of North American Class I railroads to be the most-critical engineering challenge for concrete sleepers. Shoulder/fastener wear or fatigue was identified by the same survey as the second-most-critical engineering challenge related to concrete sleepers. Lateral forces transferred through the fastening system are thought to be a primary cause of degradation of insulators. The objective of this study is to quantify the demands on the insulator through analysis of the transfer of lateral wheel loads into the fastening system by measuring the magnitude of the lateral forces entering the shoulder, a component of the fastening system adjacent to the insulator. The lateral load evaluation device (LLED) was developed at the University of Illinois in Urbana Champaign to quantify these forces. Data captured by the LLED will assist the rail industry in moving towards the mechanistic design of future fastening systems, by quantifying the lateral forces in the fastening system under representative loading conditions. Information gained through this study will also lead to a better understanding of the frictional forces at key interfaces in the fastening system. Preliminary results show that the transfer of lateral wheel loads into the fastening system is highly dependent on the magnitude of the lateral wheel loads and the frictional characteristics of the fastening system.

Keywords

Lateral force, heavy axle load, friction, concrete sleeper, fastening system

Date received: 14 November 2014; accepted: 3 September 2015

Introduction

Concrete sleepers and elastic fastening systems are typically installed in demanding loading environments, such as lines with heavy axle load (HAL) freight traffic, high degrees of curvature, steep grades, extreme climates, higher-speed rail traffic, or passenger rail traffic that requires strict geometric tolerances. These loading environments may be too demanding for conventional timber sleepers, limiting their life cycles and increasing the cost-effectiveness of concrete sleepers. Although concrete sleepers may provide a better option than conventional timber sleepers in demanding environments, they are not without their design and performance challenges. Rail seat deterioration (RSD), the degradation of the concrete material beneath the rail, has been identified through a survey of North American Class I railroads to be the most-critical engineering challenge associated with concrete sleepers. Shoulder/fastener wear or fatigue was identified through the same survey as the second-most-critical engineering challenge for concrete sleepers.[1] Shoulder/fastener wear or fatigue causes excessive rail movement, which expedites the RSD process.

The component located between the rail base and the anchorage point for the elastic clip is commonly referred to as an insulator (Figure 1). The insulator is a critical component, given that it is in contact with nearly every other component within the fastening system. However, although the insulator is a critical

Department of Civil and Environmental Engineering, University of Illinois at Urbana-Champaign, USA

Corresponding author:
J Riley Edwards, Rail Transportation and Engineering Center (RailTEC), Department of Civil and Environmental Engineering, University of Illinois at Urbana-Champaign (UIUC), 1245A Newmark Civil Engineering Laboratory, 205 North Mathews Avenue, Urbana, IL 61801, USA.
Email: jedward2@illinois.edu

component it is also designed to be a sacrificial wear component to prevent the rail or shoulder from wearing. As an insulator wears, it can lose the ability to maintain track gauge, attenuate lateral bearing forces to the shoulder, provide electrical isolation, or transmit the design clamping force from the clip to the rail. Furthermore, as an insulator wears, some track geometry defects (e.g. wide gauge) will become more prevalent and excessive rail movement can occur, accelerating the failure mechanisms of other fastening system components or the concrete sleeper itself (e.g. rail pad wear and RSD).[2,3] This presents the engineering challenge of designing an insulator that can withstand the demands at this critical interface while also maintaining the integrity of the entire fastening system.

By quantifying the lateral forces passing through the insulator and bearing on the shoulder, researchers at the University of Illinois in Urbana Champaign (UIUC) have been able to gain valuable insight into the loading demands placed on it, allowing for progression towards the mechanistic design of these fastening system components. Mechanistic design is a process derived from analytical and scientific principles, considering field loading conditions and performance requirements.[4]

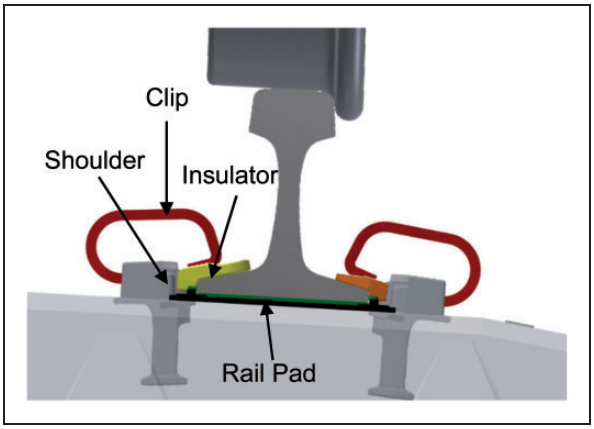

Figure 1. Component description of the Safelok I fastening system.

Measurement Technology

UIUC researchers have designed the lateral load evaluation device (LLED) to measure the lateral bearing forces acting on the shoulder and aid in the mechanistic design of the fastening system and its components. The LLED is a beam-shaped instrument that has two defined points of contact with the shoulder that act as outer supports and two defined points of contact with the insulator that are narrower than the supports. Under load, this specific geometry induces a bending action on the beam. The LLED contains four strain gauges, which are wired into a full Wheatstone bridge to measure bending strain under load. Two strain gauges are applied horizontally 1 inch from the center of the LLED to measure compressive strains (Figure 2(a)). The locations of the gauges are between the points of contact with the insulator to minimize damage to the gauges. The other two strain gauges used to measure tensile strains are applied horizontally 1 inch from the center of the LLED between the two supports (Figure 2(b)).

For installation of the instrument, the face of the shoulder of the fastening system is removed using a handheld grinder and a straight edge to ensure that the original dimensions, after placement of the LLED, are maintained (Figure 3(a) and (b)). Once the shoulder face is removed, the LLED replaces it (Figure 3(c)). Although not seen in Figure 3, a thin steel insert is placed between the insulator and the two points of contact with the LLED. This is done to ensure that the points of loading do not penetrate into the comparitively soft insulator material (Nylon 6/6). If this were to happen, it could possibly damage the strain gauge bridge, or could turn the two-point

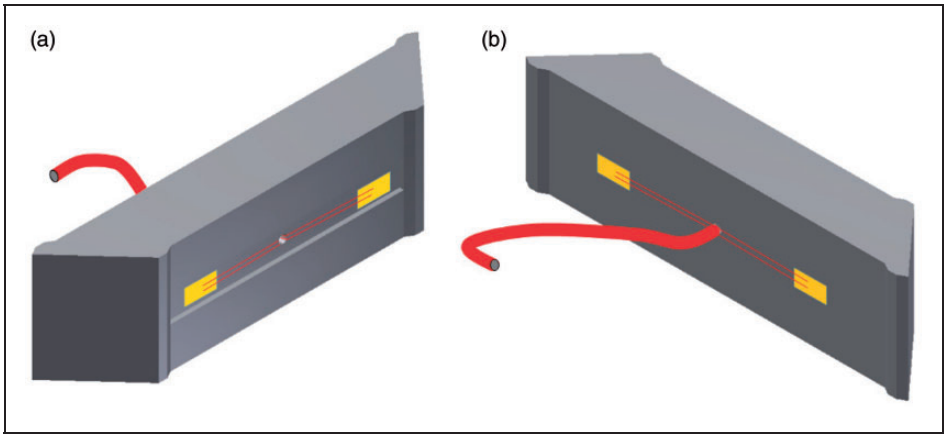

Figure 2. LLED strain gauge location and orientation.

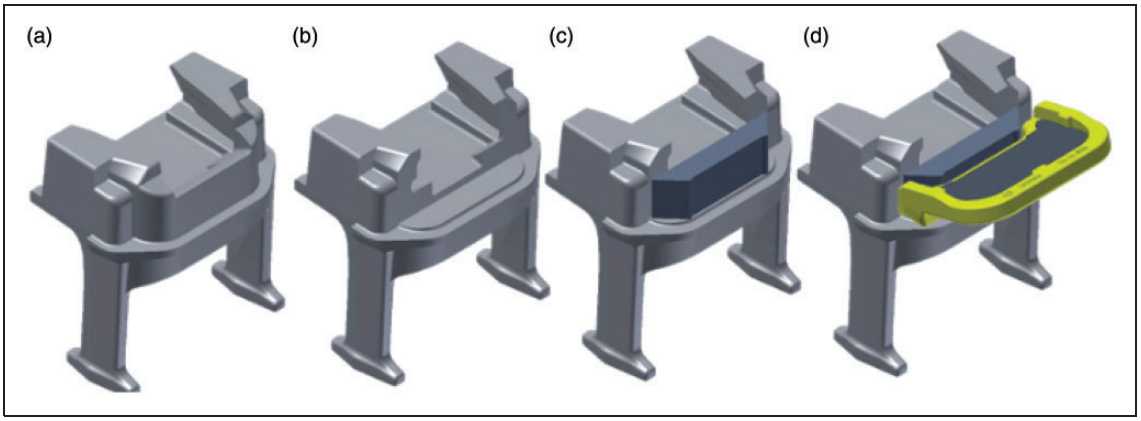

Figure 3. Isometric image showing the LLED installation process.

load into a distributed load, negatively impacting the accuracy of the results.[4]

The stiffness of the LLED and insert were chosen such that the stiffness of the system remained similar to its original condition. The primary advantage of this technology is that the original fastening system geometry is maintained, thus clip installation procedures and all fastening system components remain the same. Furthermore, material selection and geometry were also designed to reduce experimental error caused by different stiffness values from those of an unaltered fastening system. The LLED also provides researchers with the ability to understand how variables associated with friction (e.g. materials and geometry) alter the lateral load path in addition to the magnitudes of lateral fastening system forces.[5] An image of the the device on a fully installed Safelok I fastening system can be seen in Figure 4.

Calibrations of the LLEDs were conducted prior to field testing using a uniaxial loading frame. During calibration the LLEDs were supported on a plate by two small steel blocks and loaded with a self-leveling loading head to ensure perpendicular loading during calibration. Loads were applied statically in 1 kip (4.5 kN or 1000 pounds) increments with the corresponding strains being recorded from the strain gauges attached to the beam. The strains recorded from the LLEDs, along with the corresponding load applied to the instrument, were resolved into calibration curves and used to analyze data from field measurements.

Assumptions about the Lateral Load Path

Researchers at UIUC and elsewhere have succeeded in measuring and quantifying the load path in the vertical direction through the use of strain gauges and additional instrumentation in the fastening system.[6] Additionally, researchers at UIUC have successfully implemented matrix-based tactile surface sensors to measure the pressure distribution in the vertical direction at the interface of the rail pad and concrete rail seat.[7] However, there have been few

Figure 4. LLED installed in a Safelok I fastening system.

attempts to quantify and understand the mechanisms of lateral force restraint in the fastening system at a level that would guide design and maintenance practices.[8] Furthermore, the mechanisms by which lateral forces are restrained (i.e. bearing or frictional forces) are not well-understood.

For the Safelok I fastening system, it is assumed that the majority of the lateral forces from wheels are restrained by bearing forces (e.g. acting on the shoulder) and frictional forces (e.g. acting between the rail and rail pad and the rail pad and rail seat). This relationship is expressed in equation (1)

$$L_R = \Sigma L_B + \Sigma L_F + \Sigma L_r \quad (1)$$

where L_R is the total lateral restraining force, ΣL_B is the summation of the lateral bearing forces, ΣL_F is the summation of the lateral frictional forces and ΣL_r is the summation of the lateral residual forces.

All lateral bearing forces within a fastening system are measured by the LLED, as there are no other surfaces for lateral forces to bear on in a Safelok I-type fastening system. Lateral bearing restraint forces are affected by geometric tolerances within the track structure and fastening system as well as the stiffness of the lateral fastening system.[9] Lateral frictional

restraint forces occur at the interfaces between the rail and rail pad as well as the rail pad and rail seat. Lateral frictional restraint forces are affected by the vertical wheel load, material properties of the components of the fastening system, and their frictional characteristics relative to one another. The final term in equation (1), the summation of the lateral residual forces, is included to account for all minor forces acting to resist the lateral force applied to the rail. An example of these forces is the lateral resistance from the fastening system clips (both field and gauge-side clips).

Frictional forces require a force normal to the plane of the interface between two surfaces, and the relationship is expressed in equation (2)

$$L_F = \mu N \tag{2}$$

where L_F is the lateral frictional force, μ is the coefficient of friction (COF) between fastening system components (i.e. rail–rail pad, and rail pad–rail seat) and N is the force applied normal to the frictional plane (i.e. component of the vertical wheel load).

As explained by basic principles of the physics of mechanics, the friction as seen in equation (2) can be either static or kinetic, depending on the amount of force applied perpendicular to the rail seat and lateral force applied to the rail head. Static frictional forces are achieved from the interlocking of two or more surfaces to prevent any relative motion.[10] This static frictional force is present until some limit is reached, at which point motion occurs.[10] After static friction has been overcome and relative motion between the rail, rail pad, and rail seat occurs, kinetic friction is achieved. This kinetic friction typically has a lower COF than the static COF just prior to the threshold of motion. A simplified figure displaying static and kinetic friction can be seen in Figure 5.

This paper presents results from field experiments that were designed to understand the variables that affect the lateral force restraint mechanisms in the fastening system. To better understand the relationship between lateral bearing and frictional restraint forces, the following points are investigated.

1. The effect of lateral frictional restraint forces (ΣL_F) on the total lateral restraining force (L_R) by only varying the applied vertical wheel load (i.e. force applied normal to the frictional planes).
2. The percentage of total lateral restraining force (L_R) that is restrained by the lateral bearing forces, frictional forces or residual forces (ΣL_B, ΣL_F or ΣL_r) as the applied lateral wheel load increases in a three sleeper distribution
3. The lateral restraint forces under dynamic loading

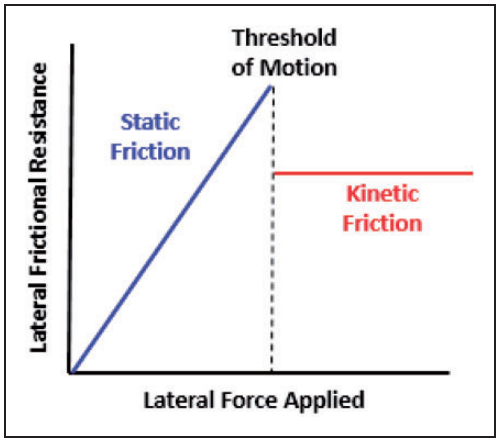

Figure 5. Simplified friction versus lateral force diagram.

Experimental setup in the field

The field experiments and results described in this paper were conducted on a segment of tangent track on the Railroad Test Track (RTT) and a segment of curved track on the High Tonnage Loop (HTL) at the Transportation Technology Center in Pueblo, Colorado. Different static loading scenarios (e.g. load magnitudes, L/V ratios, etc.) were applied to the track using the track loading vehicle (TLV) owned by the Association of American Railroads (AAR). The TLV uses a deployable axle capable of applying various combinations of vertical and lateral loads to simulate typical track-loading conditions. Although there was some variability in the contact patch between the wheel and rail, the overall benefits from this loading apparatus outweigh its limitations, as it gives researchers the ability to apply accurate single-axle loads without the effect of adjacent axles.

A HAL freight train was used to apply vertical and lateral forces under the loading conditions of the HTL at speeds of 2, 15, 30, 40 and 45 mile/h (3, 24, 48, 64 and 72 km/h, respectively). The HAL freight train consisted of three six-axle locomotives and 10 freight cars of varying weights and was used to simulate the dynamic loading of a freight train. Both test sections consisted of a 136RE rail section, concrete sleepers spaced at 24 inches (610 mm) center-to-center, Safelok I-type fastening systems, and premium ballast. Figure 6 shows the location and naming convention of the instrumentation within each test section. In each location, LLEDs were installed on the field side of three adjacent sleepers. Data were recorded at a sampling rate of 2000 Hz to accurately measure the LLED response under static and dynamic loading. All instrumentation was zeroed after installation and before any experimental data was recorded; this was in order to remove any successive forces or displacements associated with installation procedures. The measured data quantified the applied static forces from the TLV or dynamic forces from passing trains.

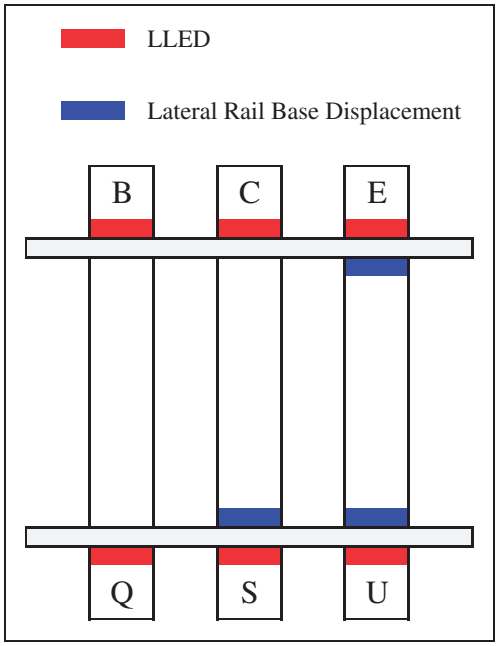

Figure 6. Instrumentation location and naming convention.

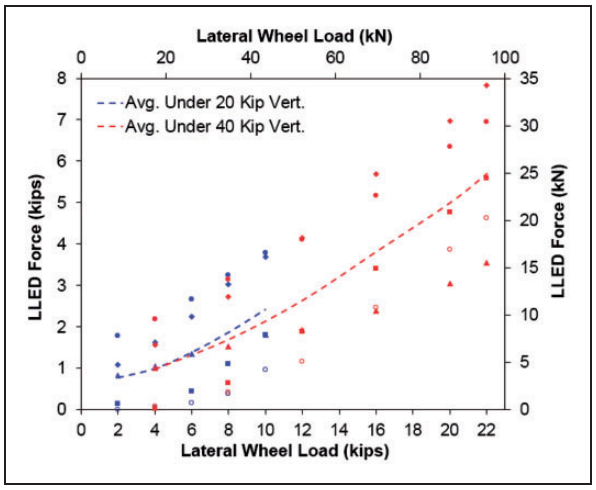

Figure 7. LLED force per rail seat as a function of lateral wheel load.

The effect of varying the applied vertical wheel load

The RTT was chosen for static testing to minimize variability due to vehicle–track dynamics in the curve. The LLED at rail seat Q on the RTT was compromised during static testing, making any data gathered from the LLED unreliable. However, rail seats B, C, E, S and U functioned properly (Figure 6). Data from the five functioning rail seats were analyzed to understand the influence of lateral wheel loads on lateral restraint forces in the fastening system. Figure 7 shows the average magnitude of the lateral bearing restraint forces measured by the LLEDs for given lateral wheel loads under constant 20 kip (89 kN) and 40 kip (178 kN) vertical wheel loads. These wheel loads were applied by the TLV directly over a specified rail seat. All data points plotted on Figure 7 from an individual rail seat are shown using a unique marker. The blue markers symbolize data collected under a constant 20 kip vertical load, and the red markers symbolize data collected under a constant 40 kip vertical load. Each data point represents a single load application to the rail and its corresponding LLED reading at five of the six rail seat locations being investigated.

The trends of the curves for 20 kip (89 kN) and 40 kip (178 kN) applied vertical wheel loads are similar. As the applied lateral wheel load increases under a constant vertical wheel load, an upward trend of lateral bearing restraint forces (i.e. forces measured by the LLED) can be seen. From the data collected during static experiments on the HTL, the difference between the average trend under 20 kip (89 kN) and 40 kip (178 kN) vertical forces appears to be negligible. The scatter of data points presented in Figure 7 may be due to varying support conditions at each rail seat and movement of the contact point of the applied load during the experiment.

As the vertical wheel load doubled, the difference between LLED forces under equivalent lateral wheel loads did not double, indicating that the frictional force did not act in the manner suggested by equation (2). This observation gives the impression that the COF-resisting applied lateral force is not constant; therefore, it is not operating in the kinetic friction range as portrayed in Figure 5. Contrary to this, analysis of lateral rail base displacement measurements taken at rail seats E, S and U showed that the rail base did move during the application of the load displayed in Figure 7. The maximum rail base displacement towards the field side under the 20 kip (89 kN) and 40 kip (178 kN) vertical load was 0.019 inches (0.483 mm) and 0.034 inches (0.864 mm) relative to the sleeper, respectively. The displacement of the rail base during the experimentation could be due to the deformation of the pad during the application of the load, or it could be due to the fact that the lateral load applied to the rail was enough to overcome the threshold of motion seen in Figure 5. Based on these observations, a reasonable conclusion cannot be drawn from Figure 7 about the effect of vertical wheel loads on both the lateral bearing and frictional restraint forces, however, it is hypothesized that slip-stick friction mechanisms between the components of the fastening system may be a contributing factor.

A similar trend regarding the effects of vertical wheel load can be seen in Figure 8. This figure shows the sum of the lateral forces from rail seats B, C and E as a function of the lateral wheel load under constant 20 kip (89 kN) and 40 kip (178 kN) vertical wheel loads applied by the TLV. In the creation of Figure 8, the assumption was made that the lateral load applied to the rail is mainly distributed into the

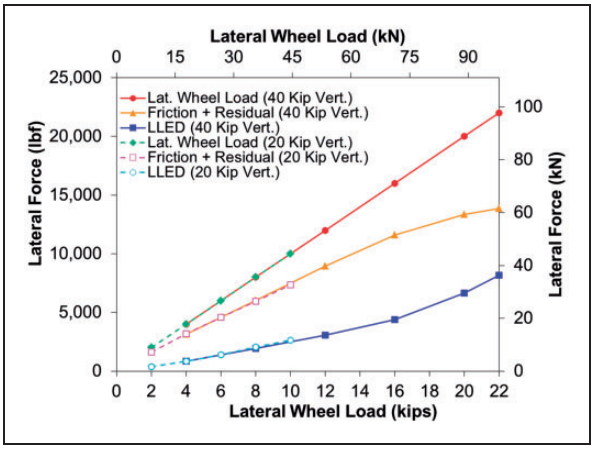

Figure 8. Sum of lateral fastening system forces on rail seats B, C and E as a function of the lateral wheel load.

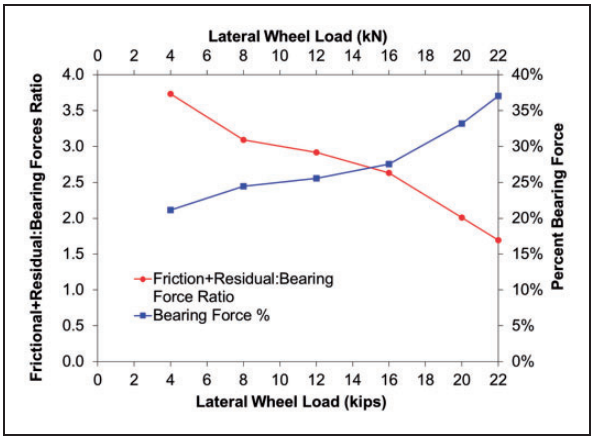

Figure 9. Change in lateral restraint forces as a function of the lateral wheel load.

three sleepers within the track structure. This assumption is based on prior research conducted at UIUC[9], which was incorporated into recent updates to the lateral load distribution section of the AREMA 2015 Manual Chapter 30. With respect to the friction and residual curves seen in Figure 8, it is assumed that the majority of this component is due to friction, however, other lateral resisting forces may also contribute to the trend. These other lateral resisting forces may include lateral resistance from the field and gauge clips. Based on equation (1) and equation (2), the difference between the lines for frictional + residual forces and bearing forces under a 20 kip (89 kN) vertical load should be smaller than that under a 40 kip (178 kN) vertical wheel load (i.e. bearing forces should increase and frictional forces should decrease). However, both 20 kip (89 kN) and 40 kip (178 kN) vertical wheel load plots appear to produce similar results for both frictional and bearing forces. Due to the uncertainty in the contribution of friction, this is an area for future research.

Percentage of lateral restraint forces

As previously mentioned, lateral frictional restraint forces are assumed to be the major contributing factor to the difference between the applied lateral wheel load and the sum of all consecutive LLEDs (i.e. lateral bearing restraint forces). As the applied lateral wheel load increases, the lateral frictional + residual forces begin to decrease and the bearing restraint forces begin to increase (Figure 8). A similar trend has also been observed through the analysis of results from UIUC's three-dimensional finite element model of the same sleeper and fastening system used in the field.[11] Figure 9 shows the change in lateral restraint forces as a function of the lateral wheel load in two ways: the ratio of frictional + residual forces to bearing forces and lateral bearing restraint forces as a percentage. As the applied lateral wheel load increases, the ratio of frictional + residual forces to the bearing forces decreases from approximately 3.7 at 4 kip (17.8 kN) of lateral wheel load to 1.7 at 22 kip (97.9 kN) of lateral wheel load, a decrease of 54%. The percentage of the applied lateral wheel load restrained by lateral bearing restraint forces increases from approximately 21% at 4 kip (17.8 kN) of lateral wheel load to 37% at 22 kip (97.9 kN) of lateral wheel load, an increase of 16%. This trend indicates that as the lateral wheel load increases, the percentage of the applied lateral wheel load restrained by lateral frictional and lateral residual forces decreases whereas the percentage of applied lateral wheel load restrained by bearing forces increases. This shows that as the lateral wheel load increases, the demands on the insulator and shoulder increase due to a higher percentage of the lateral wheel load being restrained by bearing forces.

Static versus dynamic lateral restraint forces

Figure 10 shows peak LLED forces under a HAL freight train from all axles and tested speeds as a function of the lateral wheel load. The lateral wheel loads shown in Figure 10 were collected from lateral strain bridges installed on the rail in the three sleeper instrumentation setup shown in Figure 6. The data indicate that under a 20 kip (89 kN) lateral wheel load, the lateral bearing restraint force is approximately 7000 lbf (31.1 kN) for rail seat U and 10,700 lbf (47.6 kN) when extrapolated for rail seat E. This would equate to a percentage of applied lateral wheel load restrained by lateral bearing forces of 35% and 54% for rail seats U and E, respectively. Although the data cannot be directly compared, due to different testing locations (RTT versus HTL), it can be noted that rail seat U on the low rail of the HTL behaved similarly to the averaged data from the RTT. However, rail seat E on the high rail of the HTL produced much higher magnitudes of lateral bearing forces than the remaining data. Such a high percentage

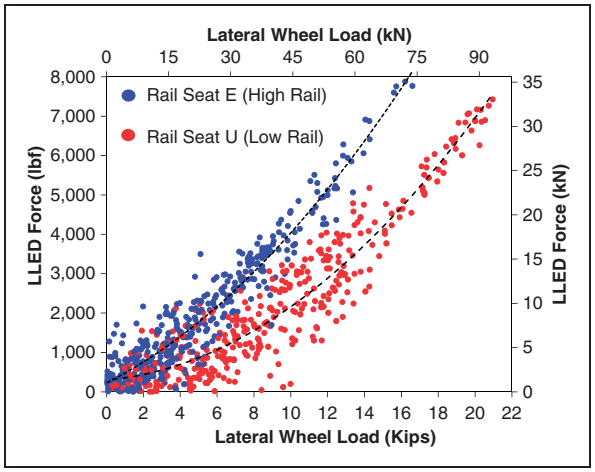

Figure 10. Peak LLED forces under a HAL freight train as a function of the lateral wheel load.

of lateral bearing forces under dynamic loads may be due to the rate of load application from the passing train and vehicle wheel–rail interaction.

Although there appears to be a correlation between lateral bearing forces and lateral wheel loads, there is still variability between the two metrics that is in need of explanation. Work has been previously conducted to understand the role friction plays on abrasion mechanisms of the concrete rail seat, as well as the role lateral fastening system stiffness plays on the magnitudes of lateral bearing forces.[9,11] Despite the research completed to date, a comprehensive understanding of the role friction plays in the transfer of lateral wheel loads into the fastening system does not exist.[9,11] This research will be continued with a stronger emphasis on the frictional characteristics of the fastening system and its effect on lateral restraint forces in concrete sleeper fastening systems.

Conclusions

This study used data collected from field implementation of the LLED to evaluate the influence of frictional characteristics and bearing forces within the Safelok I fastening system. Static observations from the field show a high degree of correlation and result in the following conclusions and observations.

1. From the experiments performed and data analyzed in this study, under equivalent static lateral loading conditions, the magnitude of the static vertical load does not seem to have a significant effect on the lateral bearing restraint forces.
2. Under a constant vertical load, as the static lateral wheel load increases, the percentage of the applied lateral wheel load restrained by bearing forces increases.

The LLED will be able to help researchers quantify the lateral restraint forces on the shoulder with minimal changes to the overall geometry of the fastening system. The creation of this device will allow researchers to better understand the lateral load path through a given fastening system, as well as the lateral load distribution through the track's superstructure. The LLED is durable enough to collect repetitive force data from a given location under the heavy haul load conditions that exist in North America, which has been a limiting factor in prior lateral load path investigations. The device has the potential to help investigate how parameters, such as friction within a given fastening system, affect the lateral load path through the track structure.

Acknowledgements

The authors would like to thank David Davis of AAR/TTCI and the members of the AAR Technology Outreach Committee: John Bosshart and Thomas Brueske of BNSF; Harold Harrison of H2 Visions, Inc.; Don Rhodes and Bill Rhodes of Instrumentation Services, Inc.; Tim Prunkard, Darold Marrow and Don Marrow of UIUC; Jose Mediavilla of Amsted RPS; Jim Beyerl of CSX Transportation; and Steve Ashmore and Chris Rewczuk of UPRR for their advice, guidance and contributions to this research. The authors would also like to thank Daniel Kuchma, David Lange, Thiago Bizarria, Christopher Rapp, Brandon Van Dyk, Sihang Wei, Justin Grasse, Kartik Manda and Andrew Scheppe from UIUC for their work on this research.

Declaration of Conflicting Interests

The author(s) declared no potential conflicts of interest with respect to the research, authorship, and/or publication of this article.

Funding

The author(s) disclosed receipt of the following financial support for the research, authorship, and/or publication of this article: This project is sponsored by a grant from the AAR Technology Outreach Program with additional funding for field experimentation provided by the United States Department of Transportation (DOT) Federal Railroad Administration. The published material in this paper represents the position of the authors and not necessarily that of DOT. J. Riley Edwards has been supported in part by grants to the UIUC Rail Transportation and Engineering Center (RailTEC) from CN, Hanson Professional Services, and the George Krambles Transportation Scholarship Fund.

References

1. Van Dyk B. *Characterization of Loading Environment for Shared – Use Railways Superstructure in North America*. Master's thesis, University of Illinois, Urbana-Champaign, 2014.
2. Hay WW. *Railroad engineering*. Second ed. New York, NY: John Wiley & Sons, 1982.
3. American Railway Engineering and Maintenance-of-Way Association. *AREMA manual for railway engineering*. Landover, MD: American Railway Engineering and Maintenance-of-Way Association, 2012 ch. 30, parts1 and 4, pp. 30–1–10.

4. Van Dyk B, Edwards JR, Ruppert CJ and Barkan CPL. Considerations for mechanistic design of concrete sleepers and elastic fastening systems in North America. In: *The International Heavy Haul Association conference*, New Delhi, India, 4–6 February 2013. Virginia Beach, VA, USA: International Heavy Haul Association (IHHA).
5. Czichos H. *Tribology: a systems approach to the science and technology of friction, lubrication and wear*. New York, NY: Elsevier North-Holland, 1978.
6. Grasse J. Field test program of the concrete crosstie and fastening system. Report, University of Illinois at Urbana-Champaign, USA, 2013.
7. Rapp CT, Dersch M, Edwards JR, et al. Measuring concrete crosstie rail seat pressure distribution with matrix based tactile surface sensors. In: TRB Editorial Board (ed.) *The Transportation Research Board annual meeting,* Washington, DC, 13–17 January 2013, pp.2–3. Washington, DC: The National Academies of Sciences, Engineering, and Medicine.
8. Rhodes D. Personal interview, 19 March 2013.
9. Williams B, Kernes R, Edwards JR and Barkan CPL. Lateral force measurement in concrete crosstie fastening systems. In: TRB Editorial Board (ed.) *The Transportation Research Board annual meeting,* Washington, DC, 12–16 January 2014, pp.8–10. Washington, DC: The National Academies of Sciences, Engineering, and Medicine.
10. Tipler PA and Mosca G. *Physics for scientists and engineers*. Sixth ed. New York, NY: W.H. Freeman and Company, 2008.
11. Chen GC, Shin M and Andrawes B. Finite element modeling of the fastening systems and the concrete sleepers in North America. <http://moodle.bcu.ac.uk/health/course/view.php?id=1356> (2013, accessed 1 March 2013).